Journal Name

ARTICLE TYPE

Cite this: DOI: 00.0000/xxxxxxxxxx

Efficiency enhancement of small molecule organic solar cells using hexapropyltruxene as an interface layer†

Hanyang Ye,*[a] Sameer Vajjala Kesava,[a] Josué F. Martinez Hardigree,[a] Roisin E. Brown,[b] Giulio Mazzotta,[a] Ross Warren,[a] Peter J. Skabara,[b‡] and Moritz Riede*[a]

Received Date
Accepted Date

DOI: 00.0000/xxxxxxxxxx

The quenching of excitons in organic solar cells can play a significant role in limiting their power conversion efficiency (PCE). In this article, we investigate the effect of a thin layer of hexapropyltruxene inserted at the interface between the electron donor boron subphthalocyanine chloride (SubPc) and its underlying hole contact in planar heterojunction solar cells. We find that a 3.8 nm hexapropyltruxene interlayer between the molybdenum oxide (MoO_x) hole contact and SubPc is sufficient to improve PCE in SubPc/C60 fullerene solar cells from 2.6 % to 3.0 %, a ∼20 % performance improvement. While the absorption stays roughly the same, the comparison of external and internal quantum efficiencies reveals a significant increase in SubPc's contribution to the current for light with wavelengths between 520 and 600 nm. Microstructure and surface morphology assessed with in-situ Grazing-Incidence Wide-Angle X-Ray Scattering (GIWAXS) and Atomic Force Microscopy (AFM), are evaluated alongside in-situ spectroscopic ellipsometry, and photoluminescence measurements. The microstructural investigations demonstrate changes to the surface and bulk of SubPc grown atop a hexapropyltruxene interlayer indicating that the latter acts as a template layer in a similar way as MoO_x. However, the improvement in PCE is found to be mainly via reduced exciton quenching at the MoO_x contact with the insertion of the hexapropyltruxene layer.

1 Introduction

Recent performance development in organic solar cells (OSCs) shows remarkable progress, achieving power conversion efficiencies (PCE) of more than 13% in single-junction devices[1–5]. Advantages such as their mechanical flexibility, portability, lightweight and potentially cost-efficient production on large area make OSCs promising alternative technology to silicon wafer-based solar cells[6,7], especially in the building-integrated PV market[7,8].

Interlayers between the photovoltaic active layer and the electrodes in OSC stacks have been studied meticulously as OSCs have developed[13,14]. They have been shown to improve the performance of the OSC devices[15,16]as well as the stability[17]. Molybdenum oxide (MoO_x) is a widely used interface modifier material in OSCs that facilitates an efficient hole contact between the anode and the photovoltaic active layer[4,5,18–21]. However, it is reported that the ITO/MoO_x anode quenches excitons generated in the active layer in OSCs if MoO_x and excitons can come into direct contact[22–24]. This quenching effect can reduce the PCE of OSCs. By inserting an interlayer between the MoO_x layer and the photovoltaic active organic layer, the quenching effect can be effectively reduced by blocking excitons from reaching the MoO_x[25]. Several small organic molecules are shown to have this effect, e.g. rubrene, TAPC, and CBP[22]. However, insertion of an additional interlayer has some side effects. A significant consequence of the insertion of interlayers is the change in morphology introduced by its template effect. Such a template layer thus can be used to influence the molecular ordering to increase the PCE of OSCs because the ordering of the molecules in the photovoltaic active layer of an OSC can have profound consequences on their performance[26–29], including improved absorption and more efficient exciton and charge carrier transport[26,30–32]. Furthermore, the energy levels of the electrode materials can also be modified by the template layer[27,33,34], which is important for device performance[33]. Research on the template growth effect has been conducted with numerous organic small molecules, e.g. perylene-derivatives[35–37], acene[38,39], phenyl- and thiophene-based molecules[40–42], and graphene/graphene oxide[43–46]. When being used, a template layer can take multiple functions in the so-

[a] Clarendon Laboratory, Parks Road, Oxford OX1 3PU, England, UK. Tel: +44-18 6528 2328; E-mail: hanyang.ye@physics.ox.ac.uk & moritz.riede@physics.ox.ac.uk
[b] WestCHEM, Department of Pure and Applied Chemistry, University of Strathclyde, Glasgow, G1 1XL, UK.

† Electronic Supplementary Information (ESI) available: [SUPPLEMENTARY INFORMATION: Efficiency enhancement of small molecule organic solar cells using hexapropyltruxene as an interface layer]. See DOI: 00.0000/00000000.

‡ Present address: School of Chemistry, University of Glasgow, Joseph Black Building. University Avenue, Glasgow, G12 8QQ, UK.

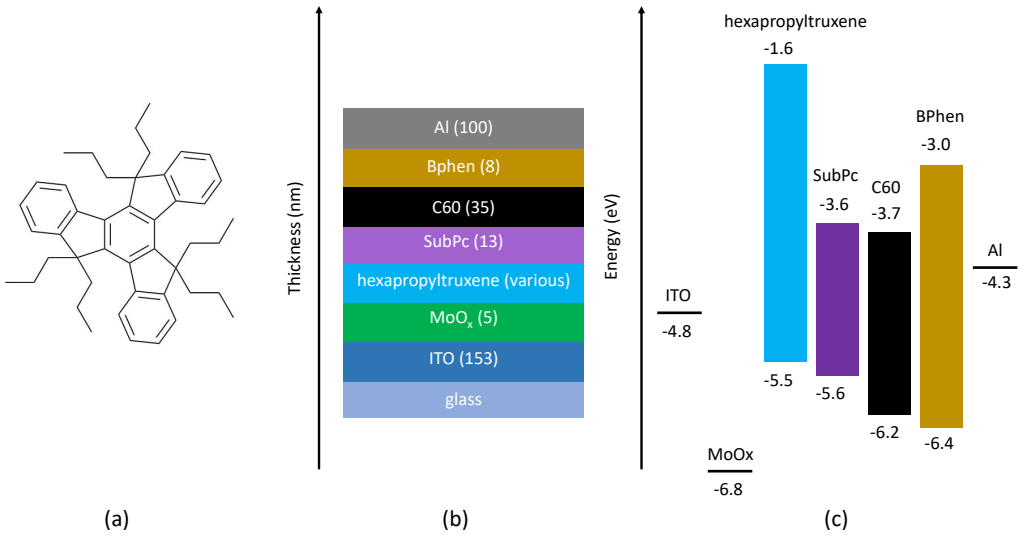

Fig. 1 Chemical structure of hexapropyltruxene, solar cell stack, and energy levels of the solar cells. (a). Chemical structure of hexapropyltruxene, (b). Schematics of the investigated solar cell stacks with the individual layer thickness given in nanometres, (c). Energy levels of materials used in this work. The indicated energy levels of SubPc (cyclic voltammetry, CV) and C60 (ultraviolet photoelectron spectroscopy, UPS & inverse photoemission spectroscopy, IPES) are taken from literature[9]. The energy levels of electrodes and MoO_x (UPS) are taken from literature[10,11]. The energy levels of BPhen (UPS) are taken from literature[12]. The HOMO-LUMO levels of hexapropyltruxene are determined by cyclic voltammetry (see SI, Figure S2).

lar cell stack, e.g. Duan *et al.* [10] reported increased OSC efficiency using a template layer which also acted as the hole transporting layer (HTL). Thus, molecules that combine this exciton blocking effect together with templating properties for the photovoltaic active layer are of high interest for OSCs.

We applied hexapropyltruxene as an interlayer between MoO_x and the photovoltaic active layer in an OSC to examine its exciton blocking effect and molecular template growth effect. Hexapropyltruxene is an alkylated derivative of the parent truxene molecule, in which the six propyl groups are positioned at the three C sp^3 sites of the compound.[47]. The chemical structure of this molecule is shown in Figure 1 (a). Truxene derivatives have been applied as photosensitizers[48], electron donor molecules[49–51], and hole transporting layers[52] in OSCs due to their good thermal stability, optoelectronic properties and ease of being modified[52–54]. Hexapropyltruxene has lower evaporation temperature in vacuum (around 100 °C at 5×10^{-7} mbar in our lab conditions) than rubrene, TAPC, and CBP (all above 150 °C), which will decrease the energy consumption in device fabrication if we replace the latter molecules with hexapropyltruxene as interlayer in OSCs. Besides, as hexapropyltruxene is nearly transparent in visible spectra (as seen in Figure S1), it will not absorb extra light to decrease the PCE of OSCs. Thus, hexapropyltruxene is a good replacement molecule to rubrene, TAPC, and CBP as interlayer inside OSCs. In-situ Grazing Incidence Wide-Angle X-ray Scattering (GIWAXS) and in-situ spectroscopic ellipsometry were used hand-in-hand to investigate the change in the growth of a SubPc layer as an electron donor after inserting the hexapropyltruxene layer. AFM measurement was performed to investigate the surface topology change. Full planar heterojunction solar cell stacks using SubPc/C60 as the photovoltaic active layer were fabricated to examine the performance change caused by insertion of the hexapropyltruxene layer. Steady-state and time-resolved photoluminescence spectroscopy (SSPL and TRPL) were carried out to evaluate the exciton quenching effect.

2 Experimental Section

2.1 Sample Fabrication

Si wafers (IDB Technologies ltd., UK), Corning Eagle XG glass substrates and ITO-coated glass substrates (both from TFD Inc., USA), were purchased commercially. The hexapropyltruxene material was synthesised following Goubard *et al.*'s report[47]. The materials for single film ultraviolet-visible spectroscopy (UV-vis) measurement had a purity of more than 95%, determined by proton Nuclear Magnetic Resonance (1H NMR). The material for cyclic voltammetry, multilayer thin film, and device fabrication was triple purified by thermal sublimation under vacuum. All organic materials (SubPc, C60, BPhen, all by Luminescence Technology Corp., Taiwan) were purchased commercially in their sublimed versions (state purity > 99%) and were used along with MoO_x (Luminescence Technology Corp., Taiwan) and Al (K. J. Lesker) as received.

We used three different vacuum chambers to fabricate our samples. They were: a multi-source bell-jar type "B30" vacuum deposition chamber (base pressure approx. 5×10^{-6} mbar, Oerlikon Leybold Vacuum Dresden GmbH, Germany) with major parts upgraded (CreaPhys GmbH, Germany). Samples fabricated in this chamber are exposed to air when being removed from the chamber for further measurements (VC-A). A multi-source vacuum deposition chamber (base pressure approx. 5×10^{-7} mbar, CreaPhys

GmbH, Germany) connected to a glovebox (LC Technology Solutions Inc., USA) where samples can be loaded from and unloaded to N_2 atmosphere without exposure to air after sample fabrication (VC-B). VC-B has an attachment specially designed for connecting an in-situ spectroscopic ellipsometer (J.A. Woollam Spectroscopic SE RC2). A small dual-source vacuum deposition chamber ("MINERVA" system, base pressure approx. 5×10^{-7} mbar, co-developed with K.J. Lesker Ltd., UK) specially designed for in-situ GIWAXS measurement (VC-C) at Diamond Light Source[55].

Substrates (glass/ITO-coated glass/Si wafer) were sonicated in 2.5% Hellmanex III soap solution, deionized water (DIW), acetone and isopropyl alcohol (IPA) each at 50 °C for 10 minutes. Subsequently, the substrates were UV-Ozone cleaned for 10 minutes before being loaded into one of the vacuum deposition chambers. Organic layers, as well as MoO_x and metal electrodes, were thermally evaporated under vacuum. The full solar cell structure (shown in Figure 1 (b), prepared in VC-B) was glass/ITO/MoO_x (5 nm, 0.1 Å/s) /hexapropyltruxene (various thicknesses, 0.1 Å/s) /SubPc (13 nm, 1 Å/s) /C60 (35 nm, 0.5 Å/s) /BPhen (8 nm, 0.8 Å/s) /Al (100 nm, 1 Å/s). The energy levels of the materials used in this solar stack are indicated in Figure 1 (c).

The fabricated devices (in VC-B) were then encapsulated with a glass cover slide (AMG Tech ltd, South Korea) and epoxy glue (UHU PLUS Endfest 2-K-Epoxidharzkleber, UHU GmbH & Co KG, Germany) in a N_2-filled glovebox for further measurements. The single layers of hexapropyltruxene were made in VC-A. The multilayers made for in-situ spectroscopic ellipsometry and photoluminescence measurements were fabricated in VC-B, multilayers made for GIWAXS and AFM measurements were made in VC-C.

2.2 Thin Film Characterization

A Cary 300 UV-vis Spectrophotometer (Agilent Technologies) was used to measure the ultraviolet-visible (UV-vis) absorbance of single hexapropyltruxene thin films.

A J. A. Woollam Spectroscopic Ellipsometer (SE RC2; J. A. Woollam, USA) system was used for the ellipsometry measurements (210 nm – 1690 nm), both for in-situ (VC-B) and ex-situ measurements as well as transmittance and reflectance measurement of thin films. In-situ measurements were carried out at an angle of 65 ° and an acquisition rate of per 10 s. CompleteEASE software (also J. A. Woollam) was used to analyze the measured data.

In-situ GIWAXS was performed during and after the growth of the films in VC-C at beamline I07 of the Diamond Light Source with a Pilatus 2M detector (Dectris AG, Switzerland) at a distance of 421 mm. The samples were fabricated on an angle-adjustable sample stage for in-situ growth observation. The incident angle of the beam on the samples was 0.15°, with a beam energy of 24 keV (wavelength λ = 0.5166 Å). The exposure time for each image was 10 s. The beam damage to the samples was avoided by laterally moving the sample area at each exposure. Data were analyzed with DAWN software[56,57]. A sector region of 15° was used to plot the line-cut profile.

Time-resolved photoluminescence measurements (TRPL) were performed with a FluoTime 300 set up (PicoQuant GmbH, Germany). The laser (generated with an LDH-P-C-510 laser diode, also from PicoQuant) wavelength was 505 nm with 128 ps pulse duration at a 10 MHz repetition rate. The excitation fluence of the laser used was ca. 20 nJ cm^{-2}. A long-wavelength pass filter was used to filter out scattered light from the excitation beam. The emission wavelengths monitored were 620 nm and 720 nm. Steady-state photoluminescence spectra (SSPL) measurements were carried out with the same instrument as the TRPL. The measuring time for each wavelength interval is 0.5 s.

For the cyclic voltammetry (CV) measurement, hexapropyltruxene, polytetrafluoroethylene (PTFE), and carbon black were mixed 1:1:1 by mass ratio to make the working electrode. Reference and counter electrodes were both lithium[58,59].

A Phillips X'pert Pro MRD was used for X-ray diffraction (XRD) measurements. The X-ray source was Cu. K-α is 1.540598 Å.

Atomic Force Microscopes (AFM) used in our experiments were an AutoProbe M5 from ThermoMicroscopes Ltd (UK) and an MFP-3D from Asylum Research (UK). Non-contact mode measurements were carried out with TAP150Al-G tips purchased from Windsor Scientific Ltd. The scanning rate was between 0.2 to 1 Hz, and the data were analyzed and processed using gwyddion software[60].

2.3 Solar Cell Performance Characterization

An Abet Class AAB solar simulator was used to perform the solar cell efficiency measurement. The solar cells were illuminated under simulated AM 1.5 sunlight. Its intensity was measured with an NREL-calibrated KG5 filtered silicon reference cell. By following a pre-established protocol[61,62], the mismatch factor for the reference solar cell without hexapropyltruxene and the solar cell with hexapropyltruxene were calculated as 0.98(0) and 0.97(7), respectively, which is close to unity. Details of the mismatch factor calculation are shown in SI, Figure S8. The dark and illuminated current-voltage (JV) curves were recorded with a Keithley 2400 Series Sourcemeter. Six solar cells in two batches (three per batch) with an active area of 7.5 mm^2 (defined by the geometric overlap between ITO and Al) were measured for each thickness of hexapropyltruxene. The exception was the stack with a 0.8 nm hexapropyltruxene layer: here, four devices from the same batch were measured, one of which had an active area of 1.5 mm^2.

The determination of the External Quantum Efficiency (EQE) was carried out using a home-made EQE set-up. Two of the best performing OSCs for each hexapropyltruxene layer thickness were measured and compared.

A UV-vis set-up consisting of a DH-2000-BAL light source, optical fibre, and a Maya Pro 2000 detector (both Ocean Optics Inc., US) was used to perform UV-vis reflectance spectroscopy. Three of the best performance OSCs with different thicknesses of interlayers were measured. Integration time was 1.168 ms, averaged over ten scans.

The Internal Quantum Efficiency (IQE) was calculated by dividing the EQE data with estimated absorption (1-R) data of each device which was measured from reflectance. This IQE measurement method is widely used and has been chosen for its simplic-

ity. Despite the known cavity effect-induced limitations[63], it still provides meaningful information to describe our system.

2.4 Model Simulation

The optical simulation was based on a transfer matrix approach[64]. Optical constants of the materials were acquired by ellipsometry measurement of thin films using the above mentioned J.A. Woollam Spectroscopic Ellipsometer (SE RC2) system.

3 Results and Discussion

The JV curves and solar cell performances are shown in Figure 2 and Figure 3, respectively. In Figure 3, the PCE of the solar cells is shown with hexapropyltruxene layer thickness systematically increasing from 0 to 3.8 nm. In this range, the PCE increases from 2.6 % to 3.0 %, mainly due to an increase in short circuit current density (J_{sc}), leading to an improvement of efficiency of about 20 %. As the thickness of the hexapropyltruxene layer is increased further from 3.8 nm to 7.7 nm, the PCE of the devices begins to drop. This is mainly due to a decrease in fill factor (FF) which changes from ca. 55 % to ca. 28 %. For all the investigated hexapropyltruxene layer thicknesses, the open-circuit voltage V_{oc} of the devices remains the same at around 1.1 V. From the JV curves (Figure 2) we can see that S-kink features are appearing when the hexapropyltruxene layer exceeds 3.8 nm. According to the shape of the S-kink in the range of 1.2 to 1.4 V, we conclude that this is an injection barrier[65–67]. Overall, we find that the PCE increase with the insertion of a hexapropyltruxene layer is mainly due to the rise of J_{sc}.

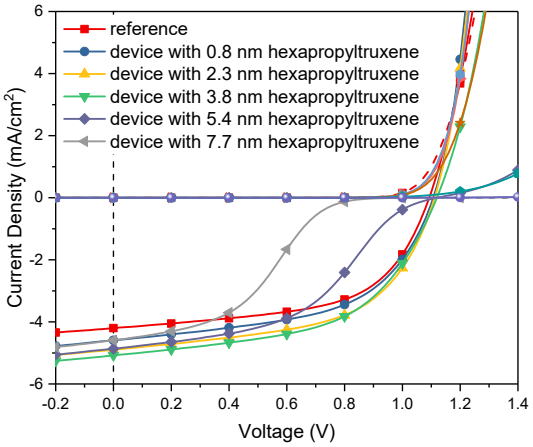

Fig. 2 JV curves of the solar cells (stack see Figure 1(b)) with different thicknesses of a hexapropyltruxene interlayer between MoO_x and SubPc. The reference device does not have a hexapropyltruxene interlayer. Solid lines are the JV curves under illumination, dashed lines are the JV curves in the dark.

To investigate the reason for the J_{sc} increases of about 25 % with the insertion of a thin layer of hexapropyltruxene, EQE and UV-vis reflectance measurement of the hexapropyltruxene solar cells with the best performance (devices with a 3.8 nm hexapropyltruxene layer) and reference devices without

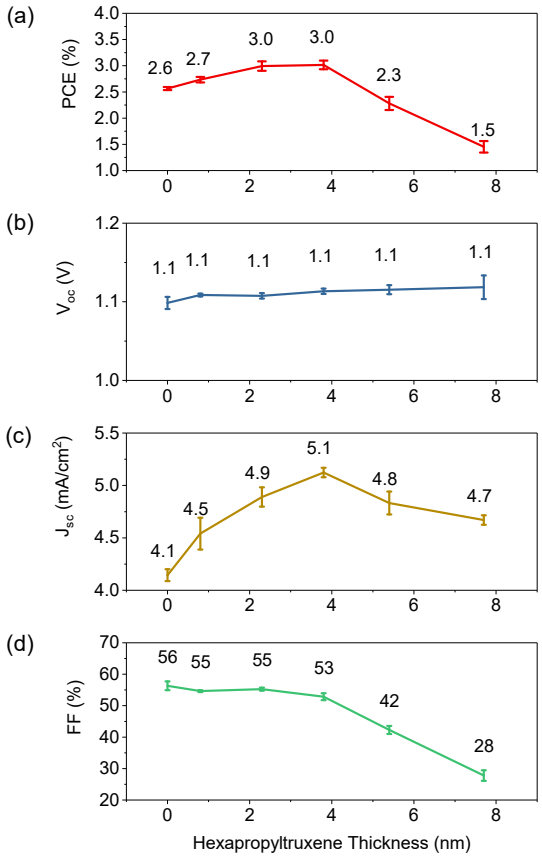

Fig. 3 Solar Cell performance versus the thickness of the hexapropyltruxene layer between MoO_x and SubPc (stack see Figure 1 a)): (a). Power conversion efficiency (PCE), (b). Open voltage (Voc), (c). Short circuit current (J_{sc}), (d). Fill factor (FF). A table of the average values and the standard deviations of photovoltaic parameters above is provided in the supporting information as Table S2.

hexapropyltruxene were carried out.

As shown in Figure 4, the EQE curves have two significant peaks: one is in the range from 330 to 400 nm (C60 absorption range), and the other is in the range from 520 to 600 nm (SubPc absorption range). The EQE of the device with hexapropyltruxene is significantly higher than the reference device in the range from about 520 to 600 nm, i.e. in the major SubPc absorption range, with the EQE peak between 520 and 600 nm, rising from 40 % (no hexapropyltruxene) to 56 % (3.8 nm hexapropyltruxene). The improvement of photocurrent generation in the range from 520 nm to 600 nm is calculated to be ca. 40 %. The estimated absorption (1- reflectivity R) of the devices as measured in UV-vis reflectance measurement shows little change in the absorption behaviour of the active layer after the insertion of hexapropyltruxene. The small absorption difference is not sufficient to explain the high increase of EQE and photocurrent generation in the SubPc absorption region. Absorption simulations of solar cell stacks with 3.8 nm/without hexapropyltruxene were carried out and shown in SI, Figure S9 and Table S1. This shows that after the

insertion of hexapropyltruxene, the light absorption of the active layer slightly changes: SubPc absorbs less light while C60 absorbs more. Calculations of the absorbed number of photons per unit area and time show that after the insertion of hexapropyltruxene, photon absorption of SubPc layer decreases from 36 % of the total absorption of the stack to 32 %, while C60 absorption increases from 30 % to 33 %. It is due to changes in the cavity and the slight shift of the light interference before and after the insertion of hexapropyltruxene. However, the total absorption of the photovoltaic active layer stays similar after the insertion of the hexapropyltruxene layer according to the simulations. Thus, the change of the absorption behaviour in SubPc and C60 layers can not account for the significant rise of EQE and photocurrent generation. We notice that this simulation result shows small difference comparing to the reflectivity measurement (estimated absorption (1-R) calculated from reflectivity measurement shown in Figure 4), which might be due to slightly different thicknesses in the measured films and simulation data. In any case, the small change in absorption behaviour of the active layer cannot explain the significant increase in EQE and photocurrent generation. Further simulations and UV-vis reflectance measurements confirm that the change in EQE is due to a corresponding change in IQE (See SI, Figure S10).

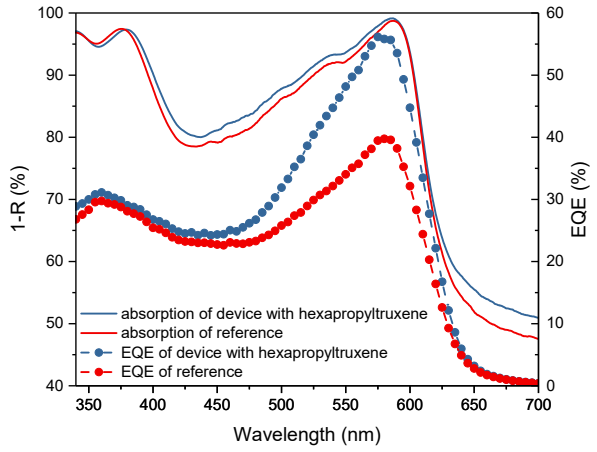

Fig. 4 External quantum efficiency (EQE) and UV-vis reflectance measurement results of reference devices without a hexapropyltruxene layer and the devices with 3.8 nm hexapropyltruxene between MoO_x and SubPc showing the best performance. R is the measured reflectance of the stack.

In order to examine the effect that the hexapropyltruxene interlayer has on the growth of the subsequent SubPc, spectroscopic ellipsometry measurements of the device stack up to the C60 layer with and without hexapropyltruxene were carried out in-situ during the deposition of the SubPc layer. The SubPc layer was modelled as a uniaxial layer, i.e. with different in-plane and out-of-plane refractive indices. The derived refractive indices, shown in Figure 5, reveal that the in-plane optical property of the stack stays similar after inserting the hexapropyltruxene interlayer, which is in line with the absorptance measurements.

The out-of-plane refractive indices, however, shows a notable

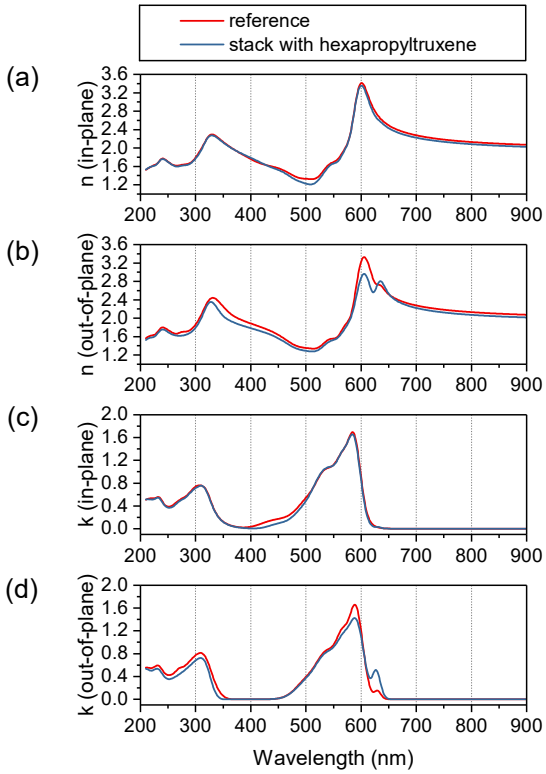

Fig. 5 In-plane and out-of-plane refractive overall indices n, k of the reference device stack (Si/MoO_x (5 nm)/SubPc (13 nm) /C60 (35 nm)) and a device stack with hexapropyltruxene (Si/ hexapropyltruxene (3.8 nm)/MoO_x (5 nm)/SubPc (13 nm)/C60 (35 nm)). (a). in-plane refractive indices n, (b). out-of-plane refractive indices n, (c). in-plane refractive indices k, (d). out-of-plane refractive indices k.

difference between the stack with hexapropyltruxene and without. For the out-of-plane refractive index k, there is a peak at 630 nm rise after the insertion of the hexapropyltruxene layer. This increase seems to come at the cost of weakening the peak at 590 nm. Similarly, for the out-of-plane refractive index n, a trade-off in peak intensities between 605 and 633 nm is observed. These changes in absorption behaviour happen in the absorption wave range of SubPc. This indicates that the insertion of the hexapropyltruxene interlayer modifies the out-of-plane optical properties of SubPc in between MoO_x and SubPc layers, which might be a consequence of the change in the molecular ordering of SubPc.

In order to corroborate these results, in-situ GIWAXS measurements were carried out using VC-C[55]. The results are shown in Figure 6. The high intensity spot around Q_{xy} = 1.6 Å^{-1} originates from the Si/SiO_2 substrate. We find a SubPc peak at around 0.7 Å^{-1}. It could be either SubPc (110) peak (0.67 Å^{-1}) or SubPc (011) peak (0.74 Å^{-1}). In SubPc single crystal structure, (110) peak is systematically absent.[68]. Thus, this broad peak could be SubPc (011) peak. Line-cut profiles (15°) in horizontal (in-plane)

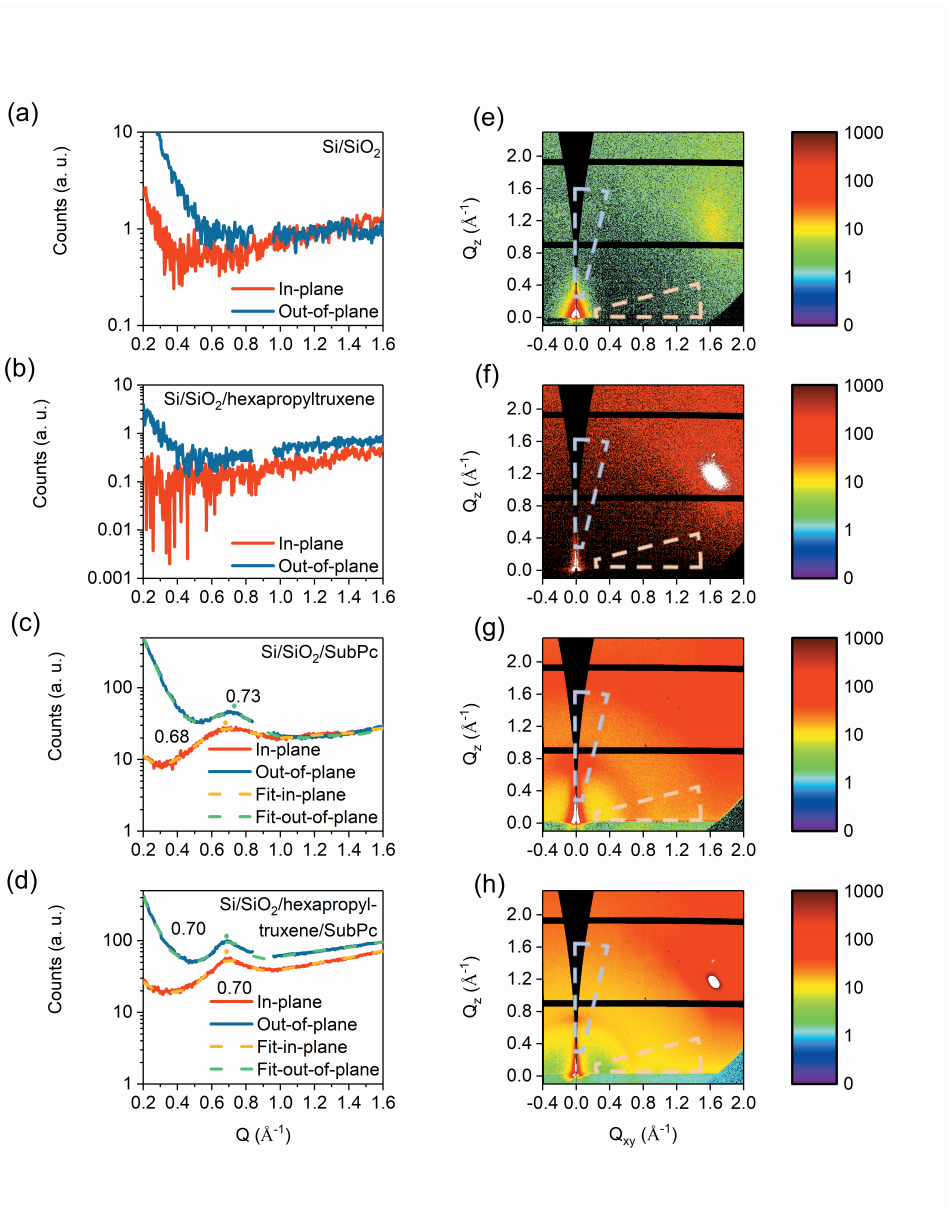

Fig. 6 Plots of the GIWAXS results obtained through measurements at Diamond Light Source's I07 beamline. In-plane and out-of-plane line cuts for (a) Si/SiO_2, (b) Si/SiO_2/hexapropyltruxene (3.8 nm), (c) Si/SiO_2/SubPc (13 nm), and (d) Si/SiO_2/hexapropyltruxene (3.8 nm)/SubPc (13 nm) multilayer films. GIWAXS images of (e) Si/SiO_2, (f) Si/SiO_2/hexapropyltruxene (3.8 nm), (g) Si/SiO_2/SubPc (13 nm), and (h) Si/SiO_2/hexapropyltruxene (3.8 nm)/SubPc (13 nm) multilayer films. Line-cut sections are indicated with dashed wedges in the figure.

and perpendicular (out-of-plane) directions were analyzed. The fitting result is shown in Figure 6 and Table 1. From the fitted full width at half maximum (FWHM) and peak maximum heights, we can find that the SubPc peak becomes sharper in both in-plane and out-of-plane directions after the insertion of hexapropyltruxene. This indicates a larger crystalline size of SubPc after the insertion of the hexapropyltruxene interlayer. The peak center locations of the SubPc (011) plane shift to 0.70 $Å^{-1}$ from 0.68 $Å^{-1}$ (in-plane) and 0.73 $Å^{-1}$ (out-of-plane) after the insertion of the hexapropyltruxene interlayer. This peak shift might be an indication of a change of crystal structure of SubPc after the insertion of hexapropyltruxene, which could explain the difference in optical properties of SubPc in the thin film. A radial distribution of the peaks is shown in Figure 7. Comparing the integrated intensities in Figure 7 between SubPc on SiO_2 and SubPc on hexapropyltruxene, we can see that the hexapropyltruxene layer affects, along with the crystallite sizes, the orientation distribution of SubPc, with a clear shoulder visible around 30 °. This affect on structure is reflected in the difference in the optical properties (Figure 5) of SubPc.

In order to complement the structural experiments, AFM measurements of SubPc layers on the relevant substrates were carried out (see SI, Figure S5). Comparing the results of the SubPc film on substrates with and without hexapropyltruxene layer, a higher roughness and shrunken surface feature size of SubPc on the hexapropyltruxene layer indicate a change in surface topology

Table 1 Fitted peak properties of the GIWAXS line cut. (Gaussian function is used in the peak fitting)

Film & orientation (*)	Peak center ($Å^{-1}$)	FWHM (δq, $Å^{-1}$)	d-value (Å)	Scherrer coherence length (D=$2\pi/\delta q$, Å)	Max height (a.u.)
Si/SiO_2/SubPc (in-plane)	0.68 ± 0.01	0.31 ± 0.01	9.24 ± 0.14	20.27 ± 0.68	12.1
Si/SiO_2/SubPc (out-of-plane)	0.73 ± 0.01	0.22 ± 0.01	8.61 ± 0.12	28.56 ± 1.36	18.8
Si/SiO_2/ hexapropyltruxene/SubPc (in-plane)	0.70 ± 0.01	0.23 ± 0.01	8.98 ± 0.13	27.32 ± 1.24	26.2
Si/SiO_2/ hexapropyltruxene/SubPc (out-of-plane)	0.70 ± 0.01	0.20 ± 0.01	8.98 ± 0.13	31.42 ± 1.65	52.8

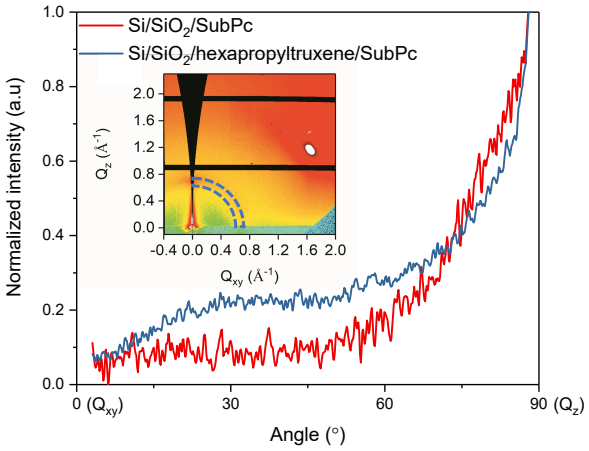

Fig. 7 Radial distribution of the GIWAXS peak from 0.65 $Å^{-1}$ to 0.75 $Å^{-1}$. The cut section is indicated with dashed sector in the inset figure. The intensities of the peaks are normalized. 0 ° stands for Q_{xy} and 90 ° stands for Q_z.

after the insertion of hexapropyltruxene interlayer. We need to point out that because of the limited organic sources in MINERVA (only two) and the conditions of the experiment at the beamtime, we were not able to perform the characterization of SubPc and hexapropyltruxene/SubPc thin film on top of MoO_x layer. Thus, this GIWAXS measurement result can only illustrate the template effect of hexapropyltruxene on SubPc, rather than the function of hexapropyltruxene layer in between the MoO_x and SubPc layer in solar cell stack, and GIWAXS data can not completely clarify the change in the ellipsometry experiment result.

To conclude the measurements, steady-state photoluminescence (SSPL) measurements were carried out and the results of the samples glass/SubPc(13 nm), glass/MoO_x (5 nm)/SubPc (13 nm), glass/hexapropyltruxene (3.8 nm)/SubPc (13 nm), and glass/MoO_x (5 nm)/ hexapropyltruxene (3.8 nm)/SubPc (13 nm) are shown in Figure 8. From Figure 8, we can see that SubPc films have two major emission peaks: around 620 and 720 nm. Comparing the PL peak intensity of bare SubPc and MoO_x/SubPc samples, we can find that the reduction of the emission peak intensity shows the exciton quenching effect of MoO_x layer. A notable increase in PL peak intensity after inserting the hexapropyltruxene layer indicates it has an exciton blocking effect. To our surprise, the peaks from glass/MoO_x/ hexapropyltruxene/SubPc have the highest intensities, even higher than the glass/hexapropyltruxene/SubPc sample. This phenomenon suggests that in addition to the exciton blocking effect from hexapropyltruxene layer, the combination of MoO_x and hexapropyltruxene layers may also affect the photoluminescence property of SubPc thin films. The reason for this change may be due to a change of the thin film structure as discussed below. Previous research illustrates that the SubPc PL emission components at these two peaks have different mechanisms. The emission component around 620 nm is reported to originate from the direct emission of excitons while the component around 720 nm comes from the emission of trapped excitons in structural defects of the SubPc films[25,69]. Because of this reason, the ratio of the peak intensities (I_{720nm}/I_{620nm}) can be used as an indication of the concentration of microstructural defects inside the SubPc layer. We calculated the peak intensity ratio of the SSPL signal for each sample (see Figure 8): SubPc 3.51, MoO_x/SubPc 1.87, hexapropyltruxene/SubPc 3.36, and MoO_x/hexapropyltruxene/SubPc 2.49. The change of ratios indicates that apart from the exciton quenching effect, MoO_x layer also seems to reduce the microstructural defects concentration inside the subsequent deposited SubPc layer. This finding suggests that MoO_x layer not only quenches the excitons inside SubPc but also modifies the SubPc film structure. The addition of hexapropyltruxene interlayer between MoO_x and SubPc layer can recover this effect. However, I_{720nm}/I_{620nm} ratio of hexapropyltruxene/SubPc sample is still slightly lower than that of SubPc sample. This may be due to the template effect of hexapropyltruxene on SubPc, which has been observed in GIWAXS measurement.

To further investigate the emission components' lifetimes, time-resolved photoluminescence (TRPL) spectra were performed for the same samples. The results are shown in Figure 9. The instrument response function (IRF) is also plotted together with the experimental results.

Considering the different mechanisms of emission components at 620 and 720 nm[69], we used a single exponential fit to calculate the exciton lifetime at 620 nm, while a bi-exponential fit was utilized to model the component lifetime at 720 nm. The fitted lifetimes of emission components are shown in Table 2. The exciton lifetimes in different samples are similar to each other, due to the intrinsic short lifetime of excitons at an excitation with 620 nm wavelength. As the emission component at 720 nm is due to trapped excitons in structural defects in SubPc, it is observed to have a longer lifetime than the emission at 620 nm. However, we still find that after inserting the MoO_x layer beneath the SubPc layer, the exciton lifetime decreases. This result agrees with the

Table 2 Time-resolved photoluminescence lifetimes of SubPc thin films on quartz glass with different interlayers. The emission component lifetime is measured at 620 nm and 720 nm.

Film	Emission wavelength (nm)	τ_1 (ns)	τ_2 (ns)	χ^2 (reduced)
glass/SubPc	620*	0.593		2.971
glass/MoO_x/SubPc		0.576		1.986
glass/ MoO_x/hexapropyltruxene/SubPc		0.674		3.729
glass/hexapropyltruxene/SubPc		0.671		3.02
glass/SubPc	720*	5.018	2.419	1.076
glass/MoO_x/SubPc		3.563	1.302	1.085
glass/ MoO_x/hexapropyltruxene/SubPc		4.786	2.116	1.036
glass/hexapropyltruxene/SubPc		5.546	2.924	1.022

* The 620 nm data sets were fitted with the single exponential model while the 720 nm data sets were fitted with the bi-exponential model.

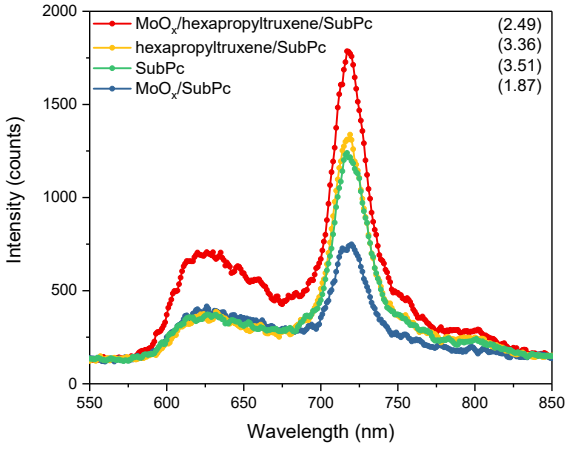

Fig. 8 Steady-state photoluminescence (PL) spectra of glass/SubPc(13 nm), glass/MoO_x (5 nm)/SubPc (13 nm), and glass/ MoO_x (5 nm)/hexapropyltruxene (3.8 nm)/SubPc (13 nm). The numers in brackets on the right side of the graph are the ratios of peak intensities (I_{720nm}/I_{620nm}) of the corresponding samples.

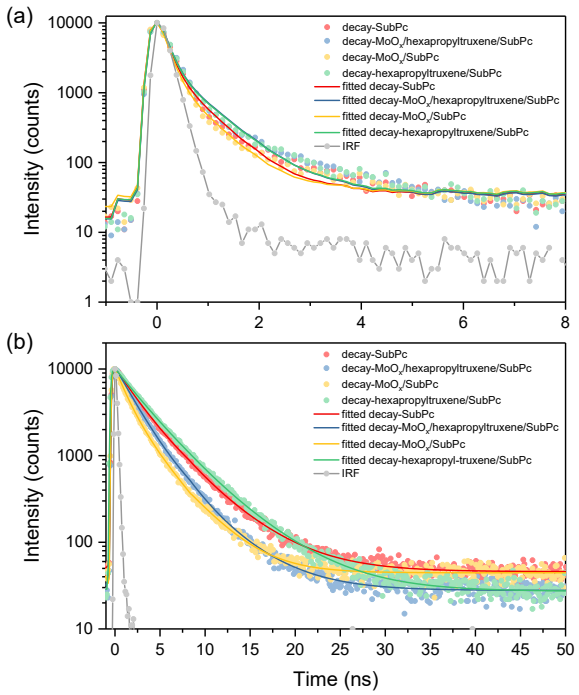

Fig. 9 Time resolved photoluminescence (TRPL) decay dynamics of glass/SubPc(13 nm), glass/MoO_x (5 nm)/SubPc (13 nm), glass/hexapropyltruxene (3.8 nm)/SubPc (13 nm) and glass/ MoO_x (5 nm)/hexapropyltruxene (3.8 nm)/SubPc (13 nm). The instrument response function (IRF) is plotted together with the sample data. (a). TRPL decay dynamics at 620 nm wavelength, (b). TRPL decay dynamics at 720 nm wavelength.

quenching effect of the MoO_x layer. The estimated quenching effect (reduction of PL emission component lifetime at 620 nm) is about 3 % calculated according to the classical diffusion equation[69,70]. After inserting the hexapropyltruxene, the exciton lifetime increases (from 0.576 ns to 0.674 ns). It improves even more than that in the bare SubPc film on glass (increases from 0.593 ns to 0.674 ns). This shows that the hexapropyltruxene layer can reduce the exciton quenching effect of the MoO_x layer. At 720 nm, the lifetime of the emission component decreases when a MoO_x layer is present directly beneath the SubPc layer compared with SubPc on bare glass. The estimated exciton quenching effect (reduction of PL emission component lifetime at 720 nm) is around 40 %. The lifetime increases again after inserting hexapropyltruxene in between MoO_x layer and SubPc layer, but it is still shorter than the ones in the pure SubPc layer (see Table 2). For the glass/hexapropyltruxene/SubPc sample, the lifetime of the emission is even longer than it is for the SubPc on glass layer. These results indicate that the hexapropyltruxene layer acts as an exciton blocking layer between MoO_x and SubPc layers. It is worth noting that the exciton/emission component lifetimes of the hexapropyltruxene/SubPc sample at both 620 and 720 nm are longer than those in the glass/SubPc sample. It may indicate that apart from the exciton-blocking effect, the small microstructural changes induced by hexapropyltruxene in the subsequent SubPc layer affects the exciton lifetime, as well. In particular, the emission at 720 nm is caused by the excitons trapped inside the

structural defects of the SubPc layer[69].

4 Conclusion

By exploring the characteristics of hexapropyltruxene and its application in standard SubPc/C60 planar heterojunction solar cells, we find that it acts as a functional interface modifier layer on top of a MoO_x hole contact layer. A maximum enhancement in PCE of about +20 % was achieved by inserting a 3.8 nm interlayer layer between MoO_x and the photovoltaic active donor layer of SubPc. Our characterization of the thin film microstructure shows that hexapropyltruxene modifies the growth of the subsequently deposited SubPc layer. In-situ GIWAXS and in-situ spectroscopic ellipsometry measurements indicate that insertion of the hexapropyltruxene layer induces a change of the crystal structure of SubPc, which impacts the absorption properties and concentration of crystal structure defects of SubPc. However, absorption changes have only a minor impact on device performance. Looking at TRPL spectroscopy, we find the enhancement of the PCE is mainly due to improved blocking of photogenerated excitons from recombining at the MoO_x interface. The excitons are trapped in the defects in SubPc films induced by the hexapropyltruxene layer, which increases the lifetime of photogenerated excitons by ca. 35 %. This shows that hexapropyltruxene can be used with beneficial effects as an interface layer in small molecule OSCs containing SubPc and potentially other 'small molecule' materials, as our results indicate that electrode modification with hexapropyltruxene may offer a practical approach for PCE enhancement.

Conflicts of interest

There are no conflicts to declare.

Acknowledgements

HY would like to acknowledge the China Scholarship Council (CSC), Pacific Alliance Group (PAG), and China Oxford Scholarship Fund (COSF) for their support. SVK and MKR acknowledge funding from EPSRC grant EP/M015173/1. JMH and MKR acknowledge funding from STFC grant ST/L006294/1 and beamtime SI18016 at Diamond Light Source. REB and PJS would like to thank the EPSRC and Cambridge Display Technology for funding. GM acknowledges EPSRC for the funding through the Centre for Doctoral Training in New and Sustainable PV (EP/L01551X/1) and University College, Oxford, for the Oxford-Radcliffe scholarship. We thank A. Warne and J. Rawle for their support with beamline instrumentation. We are grateful to J. Naylor, D. Wicks and A. Dorman of K.J. Lesker Ltd. for generously providing deposition control and evaporation sources along with technical support for MINERVA. We thank A. Ramadan, B. Wenger, N. Sakai, J. Liu, A. Privitera, and P. Kaienburg's fruitful discussions and S. Lukanihins for the program code of the optical simulation.

Notes and references

1 M. A. Green, Y. Hishikawa, E. D. Dunlop, D. H. Levi, J. Hohl-Ebinger, M. Yoshita and A. W. Ho-Baillie, *Progress in Photovoltaics: Research and Applications*, 2019, **27**, 3–12.

2 M. Shahid, Z. Fei, A. S. R. Chesman, F. D. Eisner, J. Nelson, X. Jiao, T. D. Anthopoulos, C. D. Easton, Y. Han, J. A. Röhr, C. R. McNeill, M. Azzouzi and M. Heeney, *Advanced Materials*, 2018, **30**, 1705209.

3 H. Zhang, H. Yao, J. Hou, J. Zhu, J. Zhang, W. Li, R. Yu, B. Gao, S. Zhang and J. Hou, *Advanced Materials*, 2018, **1800613**, 1–7.

4 W. Zhao, S. Li, H. Yao, S. Zhang, Y. Zhang, B. Yang and J. Hou, *Journal of the American Chemical Society*, 2017, **139**, 7148–7151.

5 X. Xu, T. Yu, Z. Bi, W. Ma, Y. Li and Q. Peng, *Advanced Materials*, 2017, **1703973**, 1703973.

6 Y. Huang, E. J. Kramer, A. J. Heeger and G. C. Bazan, *Chem. Rev.*, 2014, **114**, 7006–7043.

7 G. Li, R. Zhu and Y. Yang, *Nature Photonics*, 2012, **6**, 153–161.

8 Y.-W. Su, S.-C. Lan and K.-H. Wei, *Mater. Today (Oxford, U. K.)*, 2012, **15**, 554–562.

9 K. L. Mutolo, E. I. Mayo, B. P. Rand, S. R. Forrest and M. E. Thompson, *Journal of the American Chemical Society*, 2006, **128**, 8108–8109.

10 H. Duan, J. Yang, L. Fu, J. Xiong, B. Yang, J. Ouyang, C. Zhou, H. Huang and Y. Gao, *Thin Solid Films*, 2015, **574**, 146–151.

11 M. L. Zhang, Irfan, H. J. Ding, Y. L. Gao and C. W. Tang, *Applied Physics Letters*, 2010, **96**, year.

12 Q. Burlingame, C. Coburn, X. Che, A. Panda, Y. Qu and S. R. Forrest, *Nature*, 2018, **554**, 77–80.

13 Z. Yin, J. Wei and Q. Zheng, *Advanced Science*, 2016, **3**, 1–37.

14 Q. L. Song, C. M. Li, M. L. Wang, X. Y. Sun and X. Y. Hou, *Applied Physics Letters*, 2007, **90**, 071109.

15 M. Y. Chan, C. S. Lee, S. L. Lai, M. K. Fung, F. L. Wong, H. Y. Sun, K. M. Lau and S. T. Lee, *Journal of Applied Physics*, 2006, **100**, year.

16 K. J. Bergemann, J. a. Amonoo, B. Song, P. F. Green and S. R. Forrest, *Nano letters*, 2015, **15**, 3994–9.

17 S. M. B. Ghorashi, A. Behjat and R. Ajeian, *Solar Energy Materials and Solar Cells*, 2012, **96**, 50–57.

18 S. Tokito, K. Noda and Y. Taga, 1996, **2750**, 1–5.

19 R. Po, C. Carbonera, A. Bernardi and N. Camaioni, *Energy & Environmental Science*, 2011, **4**, 285.

20 C. Girotto, E. Voroshazi, D. Cheyns, P. Heremans and B. P. Rand, *ACS applied materials & interfaces*, 2011, **3**, 3244–7.

21 L. Cattin, F. Dahou, Y. Lare, M. Morsli, R. Tricot, S. Houari, a. Mokrani, K. Jondo, a. Khelil, K. Napo and J. C. Bernède, *Journal of Applied Physics*, 2009, **105**, 1–7.

22 F. Jin, Z. Su, B. Chu, P. Cheng, J. Wang, H. Zhao, Y. Gao, X. Yan and W. Li, *Scientific Reports*, 2016, **6**, 26262.

23 B. Verreet, R. Müller, B. P. Rand, K. Vasseur and P. Heremans, *Organic Electronics: physics, materials, applications*, 2011, **12**, 2131–2139.

24 Y. Nakayama, K. Morii, Y. Suzuki, H. Machida, S. Kera, N. Ueno, H. Kitagawa, Y. Noguchi and H. Ishii, *Advanced Functional Materials*, 2009, **19**, 3746–3752.

25 C. F. Lin, V. M. Nichols, Y. C. Cheng, C. J. Bardeen, M. K. Wei, S. W. Liu, C. C. Lee, W. C. Su, T. L. Chiu, H. C. Han, L. C.

Chen, C. T. Chen and J. H. Lee, *Solar Energy Materials and Solar Cells*, 2014, **122**, 264–270.
26 J. Yang, D. Yan and T. S. Jones, *Chemical Reviews*, 2015, **115**, 5570–5603.
27 B. P. Rand, D. Cheyns, K. Vasseur, N. C. Giebink, S. Mothy, Y. Yi, V. Coropceanu, D. Beljonne, J. Cornil, J. L. Br??das and J. Genoe, *Advanced Functional Materials*, 2012, **22**, 2987–2995.
28 Z. Wang, T. Miyadera, T. Yamanari and Y. Yoshida, 2014.
29 T. Taima, M. Shahiduzzaman, T. Ishizeki, K. Yamamoto, M. Karakawa, T. Kuwabara and K. Takahashi, *The Journal of Physical Chemistry C*, 2017, **121**, 19699–19704.
30 Z. Wang, Y. Zhou, T. Miyadera, M. Chikamatsu and Y. Yoshida, *ACS Applied Materials & Interfaces*, 2017, acsami.7b13989.
31 C. Lorch, R. Banerjee, J. Dieterle, A. Hinderhofer, A. Gerlach, J. Drnec and F. Schreiber, *Journal of Physical Chemistry C*, 2015, **119**, 23211–23220.
32 P. Sullivan, T. S. Jones, A. J. Ferguson and S. Heutz, *Applied Physics Letters*, 2007, **91**, 2005–2008.
33 A. Opitz, *Journal of Physics: Condensed Matter*, 2017, **29**, 133001.
34 Z. Wang, T. Miyadera, A. Saeki, Y. Zhou, S. Seki, Y. Shibata, T. Yamanari, K. Matsubara and Y. Yoshida, *Journal of Applied Physics*, 2014, **116**, 0–7.
35 S. W. Cho, A. Demasi, A. R. H. Preston, K. E. Smith, L. F. J. Piper, K. V. Chauhan and T. S. Jones, *Applied Physics Letters*, 2012, **100**, 1–5.
36 S. Heutz, R. Cloots and T. S. Jones, *Applied Physics Letters*, 2000, **77**, 3938.
37 K. V. Chauhan, P. Sullivan, J. L. Yang and T. S. Jones, *J. Phys. Chem. C*, 2010, **114**, 3304–3308.
38 T. Wang, T. R. Kafle, B. Kattel, Q. Liu, J. Wu and W.-L. Chan, *Scientific Reports*, 2016, **6**, 28895.
39 S. Duhm, G. Heimel, I. Salzmann, H. Glowatzki, R. L. Johnson, A. Vollmer, J. P. Rabe and N. Koch, *Nature Materials*, 2008, **7**, 326–332.
40 Y. Zhou, T. Taima, T. Miyadera, T. Yamanari, M. Kitamura, K. Nakatsu and Y. Yoshida, *Nano letters*, 2012, **12**, 4146–4152.
41 L. A. Rochford, A. J. Ramadan, D. S. Keeble, M. P. Ryan, S. Heutz and T. S. Jones, *Advanced Materials Interfaces*, 2015, **2**, 2–5.
42 A. J. Ramadan, L. A. Rochford, D. S. Keeble, P. Sullivan, M. P. Ryan, S. Jones and S. Heutz, *Journal of Materials Chemistry C: Materials for optical and electronic devices*, 2014, **3**, 461–465.
43 S. B. Jo, H. H. Kim, H. Lee, B. Kang, S. Lee, M. Sim, M. Kim, W. H. Lee and K. Cho, *ACS Nano*, 2015, **9**, 8206–8219.
44 S. Singha Roy, D. J. Bindl and M. S. Arnold, *Journal of Physical Chemistry Letters*, 2012, **3**, 873–878.
45 L. Zhang, S. S. Roy, R. J. Hamers, M. S. Arnold and T. L. Andrew, *Journal of Physical Chemistry C*, 2015, **119**, 45–54.
46 T. J. McDonough, L. Zhang, S. S. Roy, N. M. Kearns, M. Arnold, M. Zanni and T. L. Andrew, *Phys. Chem. Chem. Phys.*, 2017, **19**, 4809–4820.
47 F. Goubard and F. Dumur, *RSC Adv.*, 2015, **5**, 3521–3551.
48 X. Zong, M. Liang, C. Fan, K. Tang, G. Li, Z. Sun and S. Xue, 2012.
49 G. Zhang, F. Rominger and M. Mastalerz, *Chemistry - A European Journal*, 2016, **22**, 3084–3093.
50 E. M. Pérez, M. Sierra, L. Sánchez, M. R. Torres, R. Viruela, P. M. Viruela, E. Ortí and N. Martín, *Angewandte Chemie - International Edition*, 2007, **46**, 1847–1851.
51 A. Molina-Ontoria, M. Gallego, L. Echegoyen, E. M. Pérez and N. Martín, *RSC Adv.*, 2015, **5**, 31541–31546.
52 J. Wang, Y. Chen, M. Liang, G. Ge, R. Zhou, Z. Sun and S. Xue, *Dyes and Pigments*, 2016, **125**, 399–406.
53 A. J. Ramadan, C. B. Nielsen, S. Holliday, T. S. Jones, I. McCulloch and L. A. Rochford, *RSC Adv.*, 2016, **6**, 17125–17128.
54 Y. Kinoshita, R. Takenaka and H. Murata, *Applied Physics Letters*, 2008, **92**, 2008–2010.
55 C. Nicklin, J. Martinez-Hardigree, A. Warne, S. Green, M. Burt, J. Naylor, A. Dorman, D. Wicks, S. Din and M. Riede, *Review of Scientific Instruments*, 2017, **88**, 103901.
56 M. Basham, J. Filik, M. T. Wharmby, P. C. Y. Chang, B. El Kassaby, M. Gerring, J. Aishima, K. Levik, B. C. A. Pulford, I. Sikharulidze, D. Sneddon, M. Webber, S. S. Dhesi, F. Maccherozzi, O. Svensson, S. Brockhauser, G. Náray and A. W. Ashton, *Journal of Synchrotron Radiation*, 2015, **22**, 853–858.
57 J. Filik, A. W. Ashton, P. C. Chang, P. A. Chater, S. J. Day, M. Drakopoulos, M. W. Gerring, M. L. Hart, O. V. Magdysyuk, S. Michalik, A. Smith, C. C. Tang, N. J. Terrill, M. T. Wharmby and H. Wilhelm, *Journal of Applied Crystallography*, 2017, **50**, 959–966.
58 B.-L. He, B. Dong and H.-L. Li, *Electrochemistry Communications*, 2007, **9**, 425–430.
59 Y. Li, J. Wang, X. Li, D. Geng, M. N. Banis, R. Li and X. Sun, *Electrochemistry Communications*, 2012, **18**, 12–15.
60 D. Nečas and P. Klapetek, *Open Physics*, 2012, **10**, year.
61 American Society for Testing and Materials, 2010, **12**, 1–3.
62 V. Shrotriya, G. Li, Y. Yao, T. Moriarty, K. Emery and Y. Yang, *Advanced Functional Materials*, 2006, **16**, 2016–2023.
63 A. Armin, M. Velusamy, P. Wolfer, Y. Zhang, P. L. Burn, P. Meredith and A. Pivrikas, *ACS Photonics*, 2014, **1**, 173–181.
64 E. Centurioni, *Appl. Opt.*, 2005, **44**, 7532–7539.
65 W. Tress and O. Inganäs, *Solar Energy Materials and Solar Cells*, 2013, **117**, 599–603.
66 W. Tress, K. Leo and M. Riede, *Advanced Functional Materials*, 2011, **21**, 2140–2149.
67 W. Tress, S. Corvers, K. Leo and M. Riede, *Advanced Energy Materials*, 2013, **3**, 873–880.
68 J. D. Virdo, A. J. Lough and T. P. Bender, *Acta Crystallographica Section C Structural Chemistry*, 2016, **72**, 297–307.
69 H. Gommans, S. Schols, A. Kadashchuk, P. Heremans and S. C. J. Meskers, *Journal of Physical Chemistry C*, 2009, **113**, 2974–2979.
70 M. Pope and C. E. Swenberg, *Electronic processes in organic crystals and polymers*, Oxford University Press New York, 1999, vol. 2.